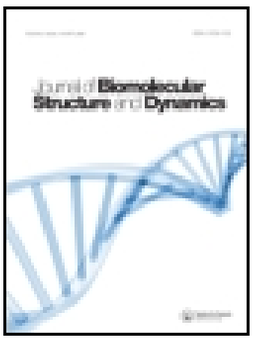

Taylor & Francis
Taylor & Francis Group

Journal of Biomolecular Structure and Dynamics

ISSN: 0739-1102 (Print) 1538-0254 (Online) Journal homepage: https://www.tandfonline.com/loi/tbsd20

Protein-Ligand Interaction Guided Discovery of Novel VEGFR-2 Inhibitors

Yanmin Zhang, Mingliang Zhang, Yuchen Wang, Yuanrong Fan, Xingye Chen, Yan Yang, Yi Hua, Wuchen Xie, Tao Lu, Weifang Tang, Yadong Chen & Haichun Liu

To cite this article: Yanmin Zhang, Mingliang Zhang, Yuchen Wang, Yuanrong Fan, Xingye Chen, Yan Yang, Yi Hua, Wuchen Xie, Tao Lu, Weifang Tang, Yadong Chen & Haichun Liu (2019): Protein-Ligand Interaction Guided Discovery of Novel VEGFR-2 Inhibitors, Journal of Biomolecular Structure and Dynamics, DOI: 10.1080/07391102.2019.1635915

To link to this article: https://doi.org/10.1080/07391102.2019.1635915

Accepted author version posted online: 24 Jun 2019.

Protein-Ligand Interaction Guided Discovery of Novel VEGFR-2 Inhibitors

Yanmin Zhang[a,1], Mingliang Zhang[b,1], Yuchen Wang[a], Yuanrong Fan[a], Xingye Chen[a], Yan Yang[a], Yi Hua[a], Wuchen Xie[a], Tao Lu[a,b,c], Weifang Tang[b], Yadong Chen[a,*] and Haichun Liu[a,*]

[a] Laboratory of Molecular Design and Drug Discovery, School of Science, China Pharmaceutical University, 639 Longmian Avenue, Nanjing 211198, China.

[b] School of Science, China Pharmaceutical University, 639 Longmian Avenue, Nanjing, Jiangsu 211198, China

[c] State Key Laboratory of Natural Medicines, China Pharmaceutical University, 24 Tongjiaxiang, Nanjing 210009, China.

[1] The authors contributed equally to this work and should be considered as cofirst authors.

*Corresponding Authors

For Haichun Liu: Tel.: +86-25-86185163. Fax: +86-25-86185182. E-mail: tuna888@126.com.

For Yadong Chen: Tel.: +86-25-86185163. Fax: +86-25-86185182. E-mail: ydchen@cpu.edu.cn.

ABSTRACT

As an effective target in abnormal angiogenesis-related tumor treatment, VEGFR-2 has small-molecule inhibitors of various scaffolds being approved for treating diseases like renal carcinoma and non-small cell lung cancer etc. However, endogenous and acquired drug resistance are still considered to be the main contributors for the failure of VEGFR-2 clinical candidates. Therefore, development of novel VEGFR-2 inhibitors is still urgently needed in the market but also challenging. In this work, residues including Asp1046, Ile1025, HIS1026, Cys919 and Lys868 were identified as the most important residues for Hbonded interaction, while His1026, Asp1046, Glu885, Ile1025 and Leu840 exhibited critical role for the nonbonded interactions through a comprehensive analysis of protein-ligand interactions, which plays critical roles in the binding of compounds and targets. Guided by the analysis of binding interactions, a total of 10 novel VEGFR-2 inhibitors based on N-methyl-4-oxo-N-propyl-1,4-dihydroquinoline-2-carboxamide scaffold were discovered through fragment-based drug design and structure-based virtual screening, which expands the chemical space of current VEGFR-2 inhibitors. Biological activity evaluation showed that even though the enzymatic activity of these compounds against VEGFR-2 were inferior to that of the positive controls sorafenib and motesanib, compound I-10 showed moderate HepG2 cell inhibitory activity with an IC_{50} value of 33.65 μM, and eight compounds exhibited moderate or higher HUVEC inhibitory activity in the range of 19.54-57.98 μM compared to the controls. Particularly, the HUVEC inhibitory activity of compound I-6 (IC_{50} = 19.54 μM)

outperformed motesanib and can be used as starting points for further optimization and development for cancer treatment.

Graphical Abstract

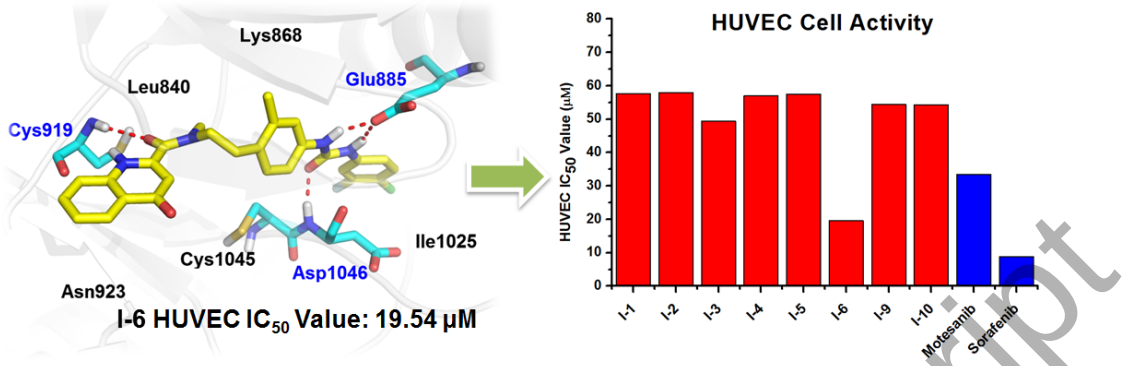

Keywords: VEGFR-2 inhibitors; Protein-ligand interaction; Fragment-based drug design; Structure-based virtual screening

1. INTRODUCTION

Angiogenesis is the formation of new blood vessels and the division of existing blood vessels(Kiselyov, Balakin, & Tkachenko, 2007). Normal angiogenesis generally occurs during ovulation, wound healing and reproduction(Klagsbrun & Moses, 1999). In the early 1970s, Folkman proposed the hypothesis that tumor growth and metastasis depend on angiogenesis, and proposed a strategy for treating cancer by inhibiting angiogenesis(Hanahan & Folkman, 1996). Since then, treating tumors by inhibiting angiogenesis has been a hot spot in the field of anticancer research(Kiselyov et al., 2007; Musumeci, Radi, Brullo, & Schenone, 2012). Later, Ferrara and colleagues found that vascular endothelial growth factor A (VEGF-A), which stimulates mitosis of endothelial cells and promotes angiogenesis(Holmes,

Roberts, Thomas, & Cross, 2007), opening the study of targets involving VEGF signaling pathways. After activation, vascular endothelial growth factor receptor (VEGFR) plays a major role in the development and progression of cancer(Ivy, Wick, & Kaufman, 2009).

When VEGF binds to VEGFR, it induces dimerization of VEGFR, causing modification of the intracellular domain. These conformational changes induce the exposure of the ATP binding site, followed by receptor dimerization upon ATP binding, resulting in the autophosphorylation or dephosphorylation of specific tyrosine residues for downstream signal transduction proteins(Koch, Tugues, Li, Gualandi, & Claesson-Welsh, 2011). Tyrosine phosphorylation on VEGFRs is regulated by internalization, degradation and dephosphorylation of different protein tyrosine phosphatases(Kappert, Peters, Böhmer, & Östman, 2005). This mechanism leads to the initiation of a typical receptor signaling cascade, which activates several downstream signal transduction pathways, such as p38-MAPK, Raf/MEK/ERK, and PI3K/PKB pathways (**Figure 1**)(Morabito, De Maio, Di Maio, Normanno, & Perrone, 2006). Activation of VEGFR and its downstream pathways will mediate cell proliferation, increase cell vascular permeability, and accelerate cell migration and cell survival, which ultimately lead to angiogenesis. Therefore, the development of inhibitors targeting VEGFR has become an important area in current anti-cancer research. Particularly, VEGFR-2 acts as a major receptor for angiogenic function, especially in tumor growth, metastasis and multidrug resistance of tumors(Ivy et al., 2009). Monoclonal antibodies or small-molecule inhibitors can block the upstream

target VEGF or VEGFR-2, and thereby inhibit the corresponding downstream pathways, resulting in the inhibition of abnormal angiogenesis (**Figure 1**)(Ivy et al., 2009).

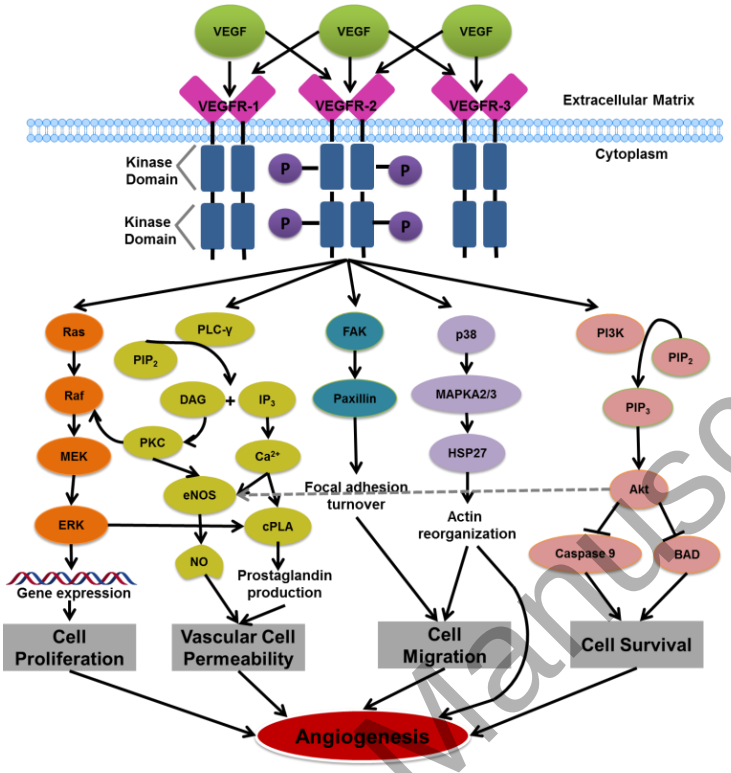

Figure 1. VEGFR signal pathways involving angiogenesis(Ivy et al., 2009).

Currently, three monoclonal antibodies including bevacizumab(Ferrara, Hillan, Gerber, & Novotny, 2004), ramucirumab, aflibercept have been approved for the treatment of metastatic colorectal cancer. Nine VEGFR-2 small-molecule drugs (**Figure 2**) including sorafenib(Folkman & D'Amore, 1996), sunitinib(Risau, 1997), pazopanib(Klagsbrun & Moses, 1999), vandetanib(Ivy et al., 2009), axitinib(Ferrara, 2004), regorafenib(Pei et al., 2006), nintenanib(Roth et al., 2009), lenvatinib(Li et al., 2006), apatinib(Roviello et al., 2016) are approved for the treatment of renal carcinoma, non-small cell lung cancer and thyroid cancer etc. in the past decades, which fully demonstrates the feasibility of treating tumors by inhibiting VEGFR-2.

Those inhibitors are all ATP competitive inhibitors(Musumeci et al., 2012), and their binding conformation with VEGFR-2 are shown in **Figure 2**. Most of those inhibitors are multi-target inhibitors with nanomolar activity for VEGFR subtypes and those targets of high sequence homology with VEGFR-2, such as PDFRR, FGFR and c-Kit etc. In addition, for VEGFR-2, there are a variety of inhibitors in clinical or preclinical studies at present, and their structures cover a wide chemical space, including quinazolines, quinolines, quinolines-2-ketones, oxindoles, phthalazines, furopyrazines, 2-aminonicotinamides, 3-aminothiophene-2-carboxamides, pyrrolotriazines, oxazoles, pyrrolopyrimidines, imidazolins, oxazolpyrrolocarbazoles and isothiazoles. Some of those compounds are previously or now in clinical I, II or III phase studies, alone or in combination for the treatment of various solid or hematoma tumors(Musumeci et al., 2012).

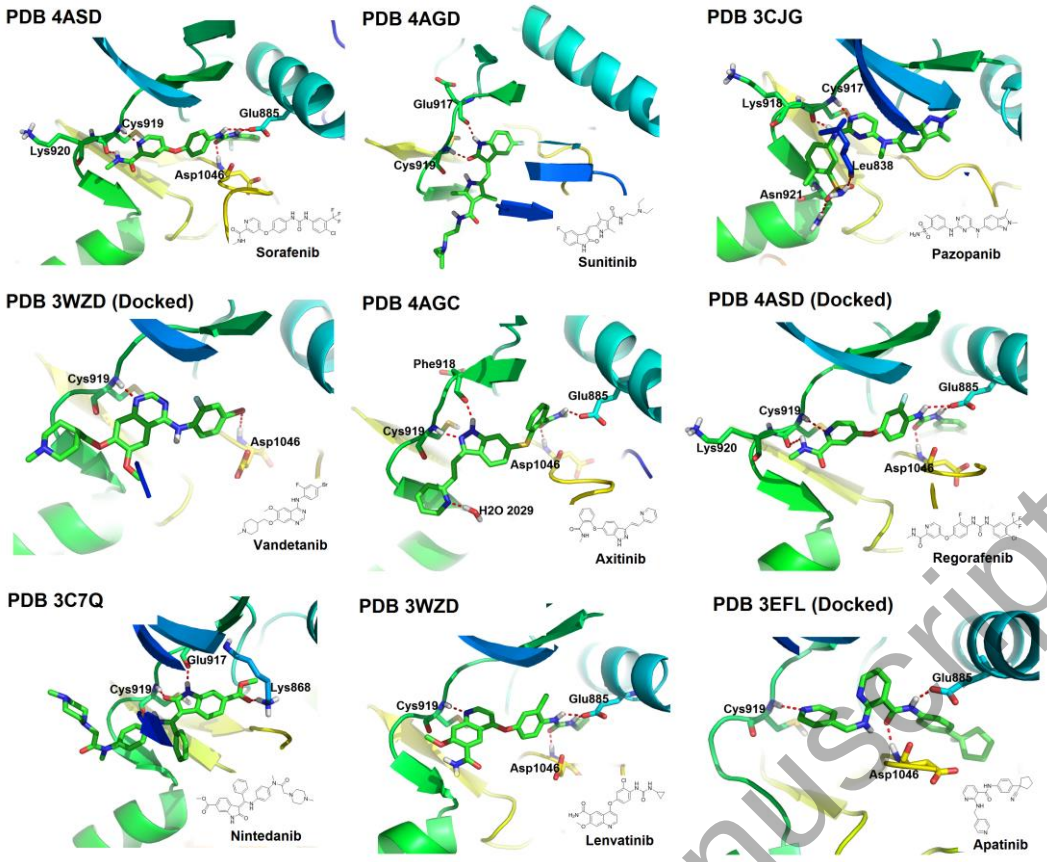

Figure 2. Binding mode of FDA approved nine VEGFR-2 inhibitors

However, whether it is bound to the active conformation of the kinase (type I) or to the inactive conformation of the kinase (type II), it is basically an ATP competitive inhibitor. Although some of these compounds are derived from minor chemical modifications to drugs that have been approved or clinically tested, most new inhibitors may be more active than their parent drugs. It is worth noting that, in addition to drug-target interactions, small changes in chemical structure can lead to different solubility or permeability, leading to strikingly different biological behaviors, especially when the target compound is a non-polar molecule, such as tyrosine kinase inhibitor. Additionally, endogenous and acquired resistance are still considered to be the main factors leading to short-term clinical effects and failure of anti-angiogenic drugs(Barouch-Bentov & Sauer, 2011; Davis et al., 2011). As various type of

VEGFR-2 inhibitors have already discovered, it is more challenging to obtain a novel hinge region scaffold. Therefore, discovering novel VEGFR-2 inhibitors with anti-angiogenic activity are still urgently needed in the market despite the challenge. Fortunately, efficient computer-aided drug design strategies offers opportunity and advantage to find promising VEGFR-2 inhibitors(Y. Zhang et al., 2017), especially the protein-ligand interaction analysis and fragment-based drug design(Bian & Xie, 2018).

In this paper, the binding cavity of VEGFR-2 and its key residues were described and summarized by analyzing the protein-ligand interaction of VEGFR-2 crystal complexes first. Then, a fragment replacement method was used to construct an in-house compound database to expand the diversity of chemical space for small molecules in virtual screening study. On the basis of the protein-ligand interaction analysis, a series of novel VEGFR-2 inhibitors with N-methyl-4-oxo-N-propyl-1,4-dihydroquinoline-2-carboxamide scaffold was obtained by structure-based screening of an in-house database and then submitted to chemical synthesis. The VEGFR-2 kinase activity and cell viability of the selected compounds were further evaluated, and several VEGFR-2 inhibitors with the novel scaffold in the hinge region were obtained, which demonstrates the application domain of protein-ligand guided discovery of kinase inhibitors.

2. MATERIALS AND METHODS

2.1 Molecular Modeling.

2.1.1 FTMAP

As a binding site detection method, FTMap samples billions of probe positions on dense translational and rotational grids based on the extremely efficient fast Fourier transform correlation approach and utilizes the sum of correlation functions for scoring.(Brenke et al., 2009) Sixteen small organic probe molecules of different hydrogen bonding capability and hydrophobicity are utilized to scan the entire surface of the protein to find the potential binding cavity. Those 16 probes consists of benzene, acetamide, ethane, acetonitrile, urea, methylamine, phenol, benzaldehyde, ethanol, isopropanol, isobutanol, acetone, acetaldehyde, dimethyl ether, cyclohexane and N,N-dimethylformamide.(Ngan et al., 2012) Any cluster with at least six probes of the lowest mean interaction energies are retained and regarded as consensus sites or hot spots. The hot spots are ranked according to the number of probes captured, with consensus site of the most probes representing the most critical sites. In addition, hydrogen bond (Hbonded) interactions and nonbonded interactions between each residue and the probes are determined. Those interactions include hydrophobic interactions, electrostatic interaction, cation π interaction, van der Waals forces, ionic interaction and etc. The frequency of probes are employed to evaluate the interactions occurred in contacting with certain residues. The online platform (http://ftmap.bu.edu)(Ngan et al., 2012) was employed for FTMap analysis.

2.1.2 Molecular Fragment Replacement

Unlike other fragment-based drug design methods, the purpose of molecular scaffold replacement is to replace part of the original molecule in an effort to maintain some of the critical binding interaction.(Bergmann, Linusson, & Zamora, 2007) The

in-house compound database was generated by MOE's scaffold replacement module(Y. Zhang et al., 2012). Crystal structure of VEGFR-2 in complexed with sorafenib (PDB 4ASD) was prepared by Protonate3D(Labute, 2009) tool to add hydrogen atoms and assign ionization states and designated as the receptor to ensure that the generated compounds can better match the binding pocket of the receptor. The lead compound was modified by deleting its hinge region part. As molecular properties are important for the discovery of druglike molecules; thus, molecular weight less than 600 D, slogP (-4 to 8), topological polar surface area (TPSA, 40 to 140) were set in the descriptor filter for finding druglike molecules (Ertl, Rohde, & Selzer, 2000; Wildman & Crippen, 1999). Through the protein-ligand interaction analysis, we learned that Cys919 is important for the binding; therefore, a one-feature pharmacophore was generated by the Pharmacophore Query tool and set as another constraint during the fragment searching phase. Finally, the Add Group to ligand module was adopted which extend a compound at one or more site to find suitable fragments for the construction of potential hits. To enrich the chemical diversity of the generated compounds, the RECAP module was used to generate more hits based on the former compound database.

2.1.3 Molecular docking

Due to its excellent performace in the virtual screening of VEGFR-2 inhibitors from our pervious study(Yanmin Zhang et al., 2013), crystal structure (PDB 3EWH) of VEGFR-2 was downloaded from the Protein Data Bank (PDB) and prepared using the Protein Preparation Wizard workflow in the Schrödinger suite(Ding et al., 2017;

Schrodinger, 2011). Water molecules beyond 5 Å of the cognate ligand were deleted and only hydrogens were selected for the restrained minimization with the force field of OPLS_2005. A grid box of similar size with the crystallized ligand was generated as the binding cavity for potential VEGFR-2 inhibitors using the Receptor Grid Generation module. The in-house database compounds were minimized by the LigPrep package(Lu et al., 2018). Because its excellent performance in a cross-docking analysis(Yanmin Zhang et al., 2013), Glide standard precision (SP) mode was chosen for molecular docking(Yanmin Zhang et al., 2013). The top 10 poses of each ligand were minimized by a post-docking procedure that saved the best pose for further analysis.

2.2 Chemistry Experiments.

Commercially available chemicals were used as purchased without further purification. Solvents were purified and stored according to standard procedures. All reactions were monitored by thin-layer chromatography (TLC), and silica gel plates with fluorescence F-254 were used and visualized with UV light. Column chromatography was carried out on silica gel (300 −400 mesh). The melting points were determined on Digital melting point instrument (Shanghai Physical Optical Instrument Factory WRS-1A) and X-4 digital display micro melting point measuring instrument (Beijing Tektronix Instrument Co., Ltd.). The NMR spectra were measured on a Bruker Avance III-300 and/or Bruker Avance III-500 instrumentment, TMS is determined by internal standard. Chemical shifts are expressed as δ units using tetramethylsilane as the external standard (in NMR description, s, singlet; d, doublet; t,

triplet; q, quartet; m, multiplet; and br, broad peak). All coupling constants (J) are reported in Hertz. MS analysis was performed on Agilent 1100 LC/MSD and 2010 GC/MS mass spectrometer (Agilent, USA). IR is SHIMADZU FTIR-8400S, KBr tablet. TLC plate is made of silica gel GF254 (produced by Qingdao Ocean Chemical Plant), ans column chromatography uses 300-400 mesh silica gel (produced by Qingdao Ocean Chemical Plant). The details of the synthesis process and structure spectra data for the target compounds as well as the intermediates can be found in the Supporting Information.

2.3 Biological Assay.

2.3.1 In vitro Kinase Assay.

One single concentration (20 μM) inhibition rate determination was entrusted to China Pharmaceutical University New Drug Screening Center. The inhibitory property on the enzyme activity was assessed by Cisbio's HTRF® KinEASE™ Kit, in which a unique substrate with a single phosphorylation site would be recognized by the phospho-tyrosine antibody labeled with the cryptate (Eu(K)). The detection reagent captures the phosphorylated substrate and the obtained homogeneous time-resolved fluorescence (HTRF) signal is in the proportion of the amount of phosphorylation.(Tardieu, 2007) Based on HTRF, the KinEASE assay consists of two steps: the first step is the kinase reaction phase and then is the detection step. 2 μL of VEGFR-2 kinase solution, 2 μL of biotin substrate and 4 μL of compound isolated in SEB-supplemented kinase buffer were added to each well for incubation in the enzymatic reaction step. For the initiation of reaction, 2 μL of LATP was then added

at room temperature (18-22°C). The reaction was carried out for 1 hour. In the second step, the detection reagents, 5 μL of tyrosine kinase antibody-Eu (K) and 5 μL of streptavidin-XL665 (SA-XL665) in EDTA, were added to each well and incubated at room temperature for 1 hour. The signal was detected using the Beckman Coulter platform HTRF detection module.

2.3.2 Anti-proliferative assay

The cell activity assessment were entrusted to Crown Bioscience Inc. Fluorescein, ATP and oxygen were treated as substrates for the luciferase in the CTG reagent to produce oxidized fluorescein and release energy in the form of light. The produced light amount is proportional to the total amount of ATP, which can reflect the total number of living cells (human umbilical vein endothelial cells, HUVEC and liver hepatocellular carcinoma, HepG2), and the fluorescence intensity is used to calculate the anti-cell proliferation rate. The method consists of several steps. The first step was cell plating, in which exponential-phase cells were collected and viable cells were counted using a Vi-Cell XR cell counting instrument. On the basis of the density in the cell culture medium, 90 μL of cell suspension was added to each well of a 96-well cell culture plate. The final cell concentration was about 2000 to 4000 cells per well (the specific cell density was regulated based on cell growth). The next step was compound partitioning, where 10 mM stock solutions in DMSO were used to dissolve target compound and these solutions were diluted 10-fold with the medium solution. 10 μL of 10-fold compound dilution in total was added to each cell line per well, resulting in a final drug concentration of 10 μM and a final DMSO concentration of

0.1%. The plates were placed in a 37 ° C incubator containing 5% CO_2 for 72 hours, followed by the plate detection step. Based on the manufacturer's instructions, 50 μL of CTG solution which was thawed previously and equilibrated to room temperature was added to each well after 72 h of drug treatment. The solution was mixed using a microplate shaker for 2 minutes. After incubation for 10 minutes at room temperature, the fluorescence signal value was measured by an Envision 2104 plate reader. Those with more than 30% cell inhibition at a concentration of 10 μM were further tested for 10 concentrations (from 10 nM to 1000 μM). Data processing: inhibition ratio=1-$V_{sample}/V_{vehicle\ control}$ *100%. V_{sample} is for drug treatment group while $V_{vehicle\ control}$ is for solvent control group. Non-linear regression models were constructed and S type dose survival curves were plotted by GraphPad Prism 5.0 software (https://www.graphpad.com/scientific-software/prism/) and the IC_{50} values were calculated. Each test was duplicated three times.

3. RESULTS AND DISCUSSION

3.1 Binding Site Analysis

The hot spots in the VEGFR-2 binding pocket were analyzed by FTMap based on a total of 38 VEGFR-2 crystal structures. **Table S1** in the Supporting Information shows the distribution of the hot spots derived from the 16 different probe types. It has been proved that the main hot spots binds at least 16 probe clusters in a druggable target and in combination with its nearby hot spots, and they constitute the binding site which potentially incorporating drug-size ligands(Dima et al., 2011; Landon, Lancia-Dr, Thiel, & Vajda, 2007; Y. Zhang et al., 2016). From **Table S1**, FTMap

could recognize at least one druggable site in all the VEGFR-2 crystal structures except for PDB 2XIR, 3CPC and 4AGC. However, they had at least four hot spots constituted by at least 10 probe clusters and their first hot spot all contained 15 probe clusters. For example, the top six hot spots for the FDA approved VEGFR-2 inhibitors crystal structures were shown in **Figure 3**, from which we could see that most of the hot spots were situated in the binding pocket of VEGFR-2 crystallized ligands. The hot spot distribution of the available VEGFR-2 crystal structures with FDA approved VEGFR-2 inhibitors consisted of 4ASD (sorafenib), 4AGD (sunitinib), 3CJG (pazopanib), 4AGC (axitinib), 3C7Q (nintedanib) and 3WZD (lenvatinib). The hot spot distributions of the other 36 VEGFR-2 complexes demonstrated similar distributions as crystal structures complexed with the FDA approved VEGFR-2 inhibitors.

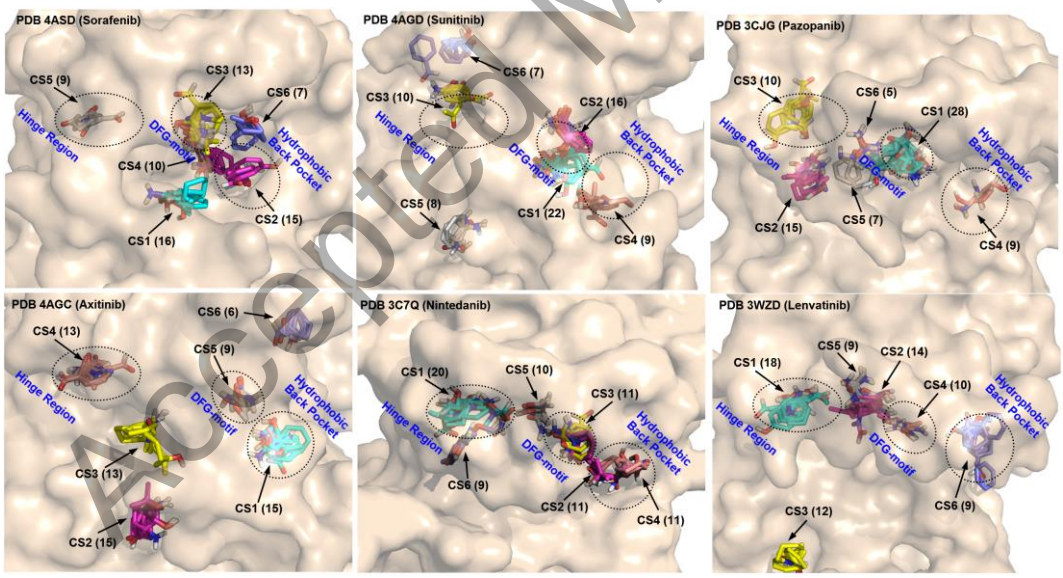

Figure 3. The top six consensus sites (CS) detected by FTMap for crystal complexes of six marketed VEGFR-2 inhibitors. CSs are denoted as lines with CS1 (cyan), CS2 (magenta), CS3 (yellow), CS4 (salmon), CS5 (gray), and CS6 (slate blue)

successively in descending number of probe clusters. The number in the parentheses is the number of probe clusters detected in that hot spot.

As shown in **Figure 3**, the binding cavity of VEGFR-2 can be generally divided into three major parts consisting of the hinge region, DFG-motif and hydrophobic back pocket. The hinge region and the hydrophobic back pocket obtained at least one consensus sites (CS), individually. According to **Table S1**, sites at PDB 3C7Q and 3WZD hinge region were all CS1, with 20 and 18 probe clusters captured, respectively. In PDB 4AGD and 3CJQ, CS1s of 22 and 28 probe clusters were located in the DFG-motif region while for PDB 4AGC, CS1 of 15 probe clusters was found in the hydrophobic back pocket. These results indicated the importance of this region, and further confirmed that the type II kinase inhibitors generally have better activity and selectivity and the DFG-motif region is an essential part for the binding of type II inhibitors for most kinase targets. Still, some consensus sites such as CS5 of 8 probe clusters in PDB 4AGD, CS3 of 13 probe clusters, CS2 of 15 probe clusters and CS6 of 6 probe clusters in PDB 4AGC, CS3 of 12 probe clusters in PDB 3WZD were situated in the wide range of the binding pocket, demonstrating the potential of sites to expand and optimize the current VEGFR-2 inhibitors. In summary, the FTMap binding site detection can accurately probe the binding pocket of VEGFR-2 and can be used as a confirmation for potential binding sites.

3.2 Protein-Ligand Interaction Analysis

Hitherto, a total of 38 VEGFR-2 crystal structures (PDB) were resolved with various types of VEGFR-2 inhibitors(Yanmin Zhang et al., 2013). A comprehensive

analysis of the protein-ligand binding interaction was conducted by detecting all the VEGFR-2 crystal structures. Herein, the frequency of both Hbonded and nonbonded interactions (**Figure 4**) for each residue in the 38 PDB complexes were calculated. **Figure 5** and **Figure 6** show the hot map of the Hbonded and nonbonded interactions, respectively. The corresponding values of the Hbonded and nonbonded interactions frequency can be found in the Supporting Information **Table S2** and **S3**. From **Figure 4** and **Figure 5**, 13 residues indicated Hbonded interaction with the cognate ligand in more than 30 PDB complexes. They were Cys919 (38/38), Leu840 (33/38) in the hinge region; Cys 1045 (36/38), Asp1046 (38/38), Glu885 (37/38), Lys868 (37/38) around the DGF-motif region; Ile1025 (36/38), His1026 (34/38), ARG1027 (33/38), ASP1028 (35/38) in the hydrophobic back pocket; and Asn923 (38/38), Ser925 (31/38), Arg1032 (38/38) within the solvent accessible region.

VEGFR-2 inhibitors are generally classified as type I (DGF-in) and type II (DGF-out) class. From the crystal complexes analysis, it can be seen that the type I inhibitors such as axitinib (PDB 4AGD) and sunitinib (PDB 4AGC) generally bind to the above key residues in the hinge region and the solvent accessible region. The type II inhibitors such as sorafenib (PDB 4ASD), lenvatinib (PDB 3WZD), and apatinib (PDB 3EFL) mainly bind to key residues in the hinge region and the hydrophobic back pocket. In addition, at least 20 PDB complexes obtained Hbonded binding interactions with residues Arg842, Ala881, Val899, Glu917, Arg929, Cys1024, Asn1033, Ile1044, Phe1047, Gly1048, Leu1049, Ala1050, Arg1066, Tyr1082, Glu1097, Ala1103 and Ser1104 within the binding pocket of VEGFR-2. Among all

residues, Lys868 (16/38), Glu885 (13/38), Cys919 (16/38), Ile1025 (29/38), His1026 (23/38), Arg1027 (14/38), Cys1045 (13/38), and Asp1046 (35/38) appeared in at least 10 PDB crystal structures with the percent of Hbonded interactions frequency higher than 5%. The results of nonbonded interaction showed similar trend with the Hbonded interaction analysis. As shown in **Figure 4** and **Figure 6**, the same 13 residues showed nonbonded interactions with their cognate ligands in at least 30 PDB complexes as compared to the Hbonded interaciton. Except Cys1045 (36/38) and ASP1046 (38/38) were slightly different with the Hbonded interactions, the other 11 residues exerted nonbonded interactions in the same number of PDB complexes. Similarly, Leu840 (10/38), Glu885 (16/38), Cys919 (4/38), Ile1025 (11/38), His1026 (27/38), Asp1046 (18/38) showed nonbonded interactions with cognate ligands in at least 10 PDB complexes. In summary, for the contributon of Hbonded interaction, Asp1046, Ile1025, HIS1026, Cys919 and Lys868 were the most important residues while His1026, Asp1046, Glu885, Ile1025 and Leu840 exhibited the most evident nonbonded interactions.

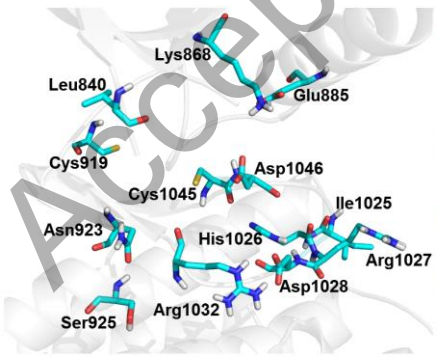

Residue	Hbonded Frequency			Nonbonded Frequency		
	>0	>5%	>10%	>0	>5%	>10%
LEU840	33	0	0	33	10	1
LYS868	37	16	5	37	4	0
GLU885	37	13	1	37	16	0
CYS919	38	16	9	38	4	0
ASN923	38	3	0	38	1	0
SER925	31	1	0	31	0	0
ILE1025	36	29	13	36	11	0
HIS1026	34	23	6	34	27	2
ARG1027	33	14	5	33	9	0
ASP1028	35	1	0	35	3	0
ARG1032	38	11	2	38	2	0
CYS1045	36	13	8	35	9	0
ASP1046	38	35	25	37	18	0

Figure 4. key residues detected from FTMap Hbonded and nonbonded analysis (PDB 3WZD) and the number of residues with a certain percent of frequency.

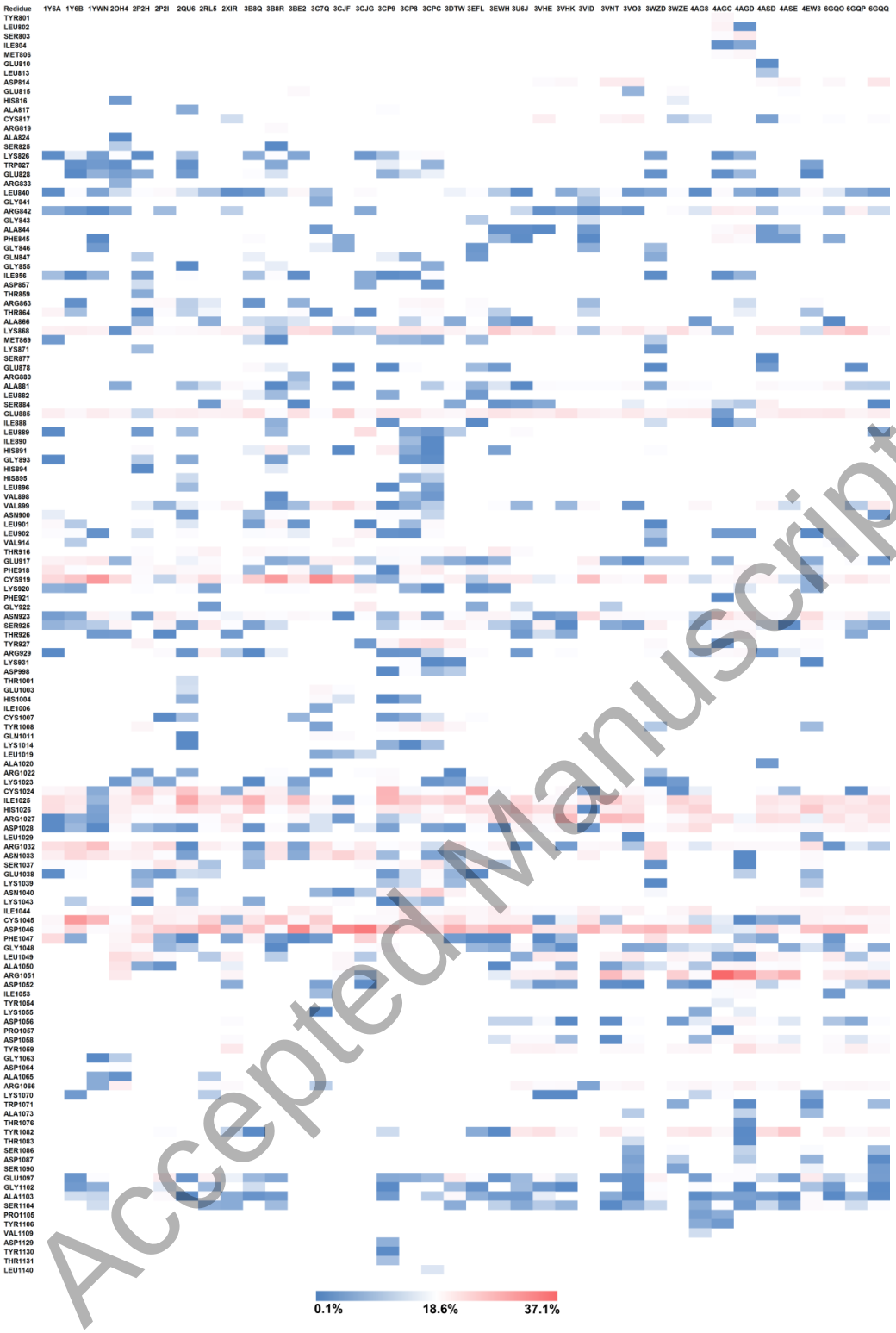

Figure 5. FTMap Hbonded interaction analysis of VEGFR-2 crystal structures.

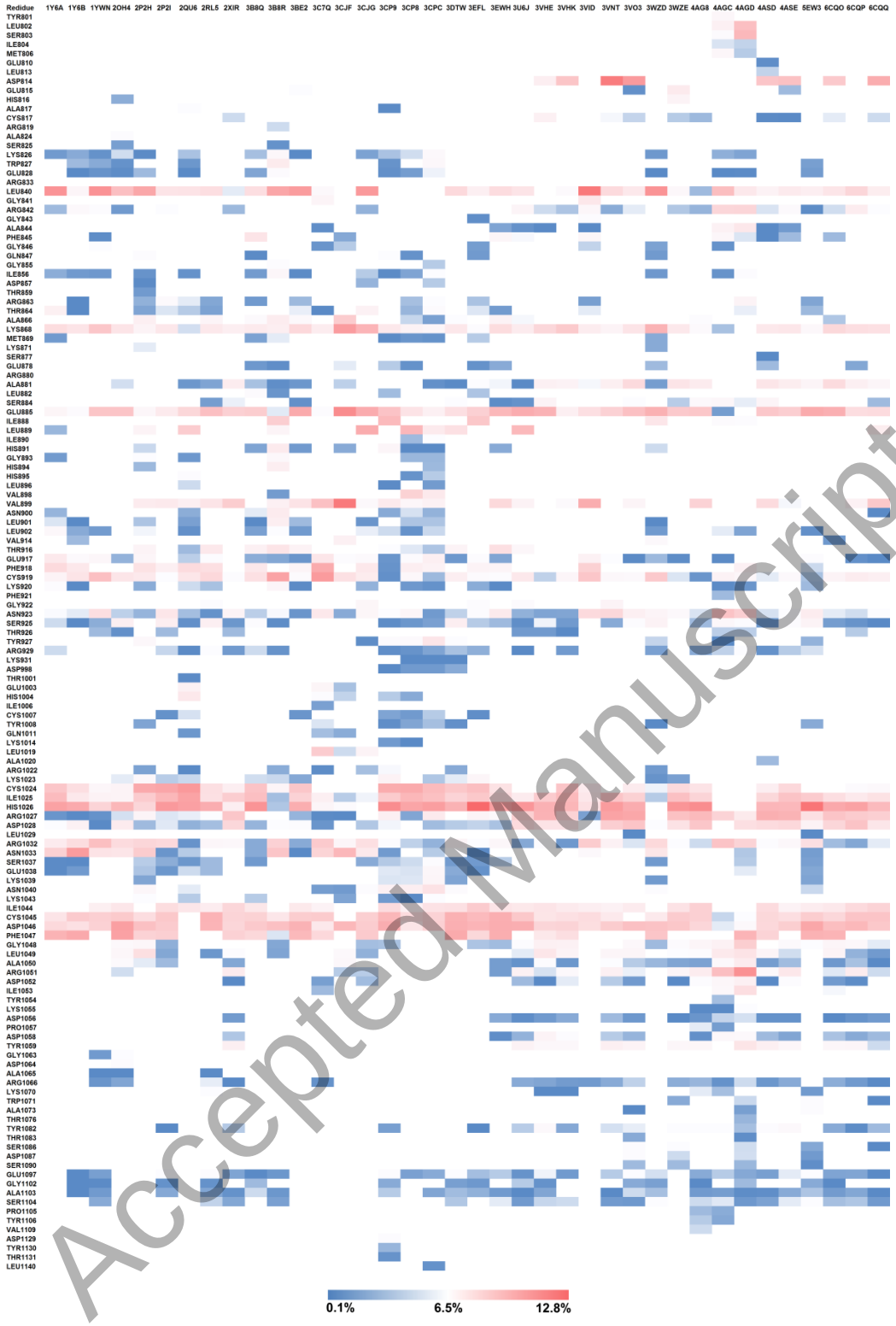

Figure 6. FTMap nonbonded interaction analysis of VEGFR-2 crystal structures.

The specific Hbonded and nonbonded interactions between the cognate ligands with representative VEGFR-2 crystal structures were shown in **Figure 7**. **Figure 7** showed the available PDBs crystallized with six FDA approved VEGFR-2 inhibitors

including sorafenib (PDB 4ASD), sunitinib (PDB 4AGD), pazopanib (PDB 3CJG), axitinib (PDB 4AGC), nintedanib(PDB 3C7Q) and 3WZD (lenvatinib). Among the six listed inhibitors, sorafenib (PDB 4ASD) and lenvatinib (PDB 3WZD) are belong to the type II kinase inhibitors as they both occupy the back hydrophobic pocket once the DFG-motif is in the out conformation. They shared similar distributions in the Hbonded and nonbonded interactions. Specifically, in terms of the Hbonded interaction frequency, for PDB 4ASD, residues with the top five highest Hbonded interaction frequency were Arg1051 (14.2%), Asp1046 (9.6%), Tyr1082 (8.7%), Arg1027 (8.4%) and Ile1025 (6.9%). For PDB 4AGD, the corresponding residues were Arg1051 (29.2%), Tyr1059 (8.0%), Ser803 (5.6%), Arg842 (4.2%) and Asn923 (3.8%). While for PDB 3CJG, the top five highest Hbonded interaction frequency were Asp1046 (33.0%), Phe1047 (11.2%), Leu889 (8.2%), Asn1033 (6.4%) and Arg1032 (5.1%). For PDB 4AGC, Arg1051 (37.1%), Asn923 (8.2%), Arg1027 (7.1%), Arg842 (4.8%) and Leu802 (3.4) ranked the top five for the Hbonded interaction frequency. In terms of PDB 3C7Q, the corresponding top five residues were Cys919 (28.3%), Lys868 (9.6%), Arg1032 (7.9%), Asp1046 (7.3%) and Asn1033 (6.2%) while for PDB 3WZD, residues with the top five highest Hbonded interaction frequency consisted of Asp1046 (17.9%), Cys919 (116.3%), Asn1033 (9.0%), Arg1032 (8.8%) and Phe 1047 (8.0%). Generally, residues with higher Hbonded interaction frequency also obtained relatively higher nonbonded interactions frequency. However, there was one exception. Even through Leu840 did not achieve high Hbonded interaction frequency as no PDBs appeared in the top five, its

nonbonded interactions frequency were relatively greater than other residues. The corresponding nonbonded interactions frequency for Leu840 were 4ASD (1.7%), 4AGD (2.4 %), 3CJG (8.9%), 4AGC (5.9%), 3C7Q (1.2%) and 3WZD (9.4%), respectively.

Overall, in the top five Hbonded interaction frequency, Cys919 in the hinge region only appeared in PDB 3C7Q (28.3%) and 3WZD (16.3%) whereas Asp1046 in the DFG-motif appeared in four PDBs including PDB 3C7Q (7.3%), 3CJG (33.0%), 3WZD (17.9%) and 4ASD (9.6%). Despite that Asp1046 in PDBs 4AGC and 4AGD did not got any top five Hbonded interaction frequency, their cognate ligands have a strong Hbonded interaction with Arg1051 of Hbonded interaction frequency of 37.1% and 29.2%, respectively. In addition, Arg1032, Asn1033 and Phe1047 were also quite critical as they appeared in at least two PDBs in the ranking of top five Hbonded interaction frequency. Moreover, the other 32 PDBs (**Figure 5** and **Figure 6**) showed similar trend with the six PDBs complexed with FDA approved drugs in terms of both Hbonded and nonbonded interaction frequencies (**Figure 7**). In total, Asp1046, Cys919, Arg1051, Phe1047, Arg1032, Asn1033 were the most important residues forming interactions with the approved VEGFR-2 inhibitors, which was consistent with previous results on the detected interactions for all VEGFR-2 crystal structures.

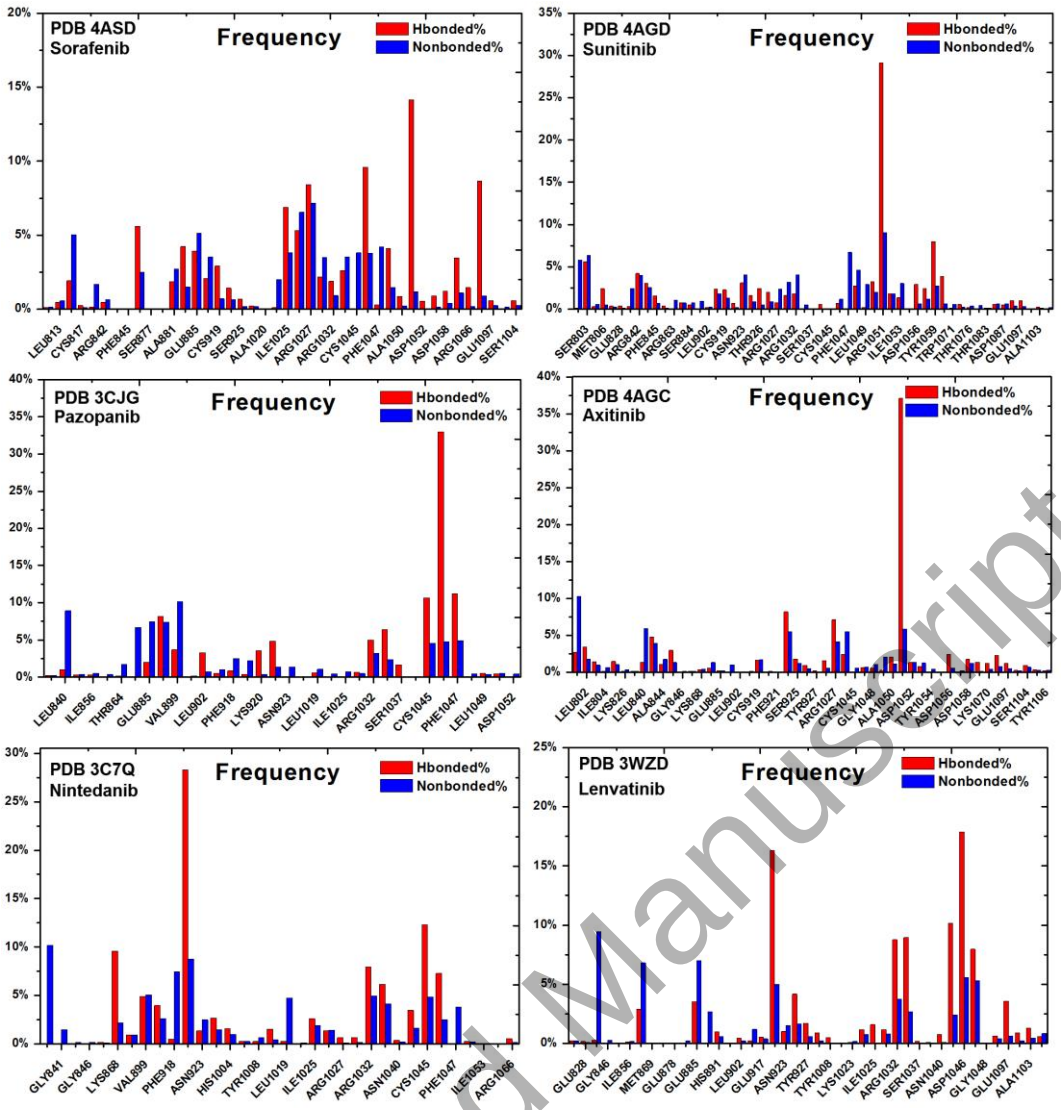

Figure 7. Hydrogen bond frequency maps in the six proteins crystal complexes of six marketed VEGFR-2 inhibitors. The red bar and blue bar represent the Hbonded interactions (Hbonded %) and the nonbonded interactions (Nonbonded %), respectively.

3.3 Structure-Based Virtual Screening

Fragment-based drug design generally includes fragment growing, fragment linking and de novo drug design(Bian & Xie, 2018). Molecular scaffold replacement belongs to fragment growing as it retains part of the known inhibitors either in the hinge region or the other pocket such as the DFG motif or the hydrophobic back pocket in

the kinase targets. Due to its relatively conserved strategy, the successful rate is higher than fragment linking and de novo drug design. The design and optimization of the lead compound is shown in **Figure 8A**. In the first step of the workflow, hinge region scaffold 4-hydroxy-N-methylpicolinamide of sorafenib was replaced by retaining the diphenylurea part which occupys the DFG motif and the hydrophobic back pocket. A total of 15595 compounds were generated by this module. After duplication, 14777 compounds were kept for later evaluation. Then, the generated compounds were submitted for molecular docking, which can explore the best binding mode between the target (here is VEGFR-2) and the target compounds and give a comprehensive docking score. PDB 3EWH was used as the receptor as it was selected as the most foavorable crystal structure for VEGFR-2 docking-based virtual screening by a comprehensive self-docking and cross-docking analysis(Yanmin Zhang et al., 2013). Third, through the protein-ligand interaction analysis, we learned that Asp1046, Ile1025, HIS1026, Cys919 and Lys868 and Leu840 were key residues responsible for Hbonded or nonbonded interactions. Thus, only the docked compounds having either Hbonded or nonbonded interactions with Asp1046, Ile1025, HIS1026, Cys919, Lys868, Leu840 and His1026 were kept for the last manually selection step. Among them, a novel scaffold in the hinge region of N-methyl-4-oxo-N-propyl-1,4-dihydroquinoline-2-carboxamide was obtained. Furthermore, as our former study(Yang et al., 2015) showed that the R_1, R_2 and R_3 sbustituents can be replaced by halogen (F, Cl, CH_3 or CF_3) to adjust the physiochemical properties, a total of 10 compounds were finally designed for further

evaluation (**Table 1**). Additionally, rather than specifically affecting one desired target, pan assay interference (PAINS) compounds are often regarded as false positives as they tend to react with numerous biological targets simultaneously.(Baell & Holloway, 2010) Thus, the designed 10 compounds were submitted to PAINS remover (http://cbligand.org/PAINS/)(Baell & Holloway, 2010) to avoid any false positives. Fortunately, all 10 compounds passed the PAINS filtration process and were adopted for chemical synthesis.

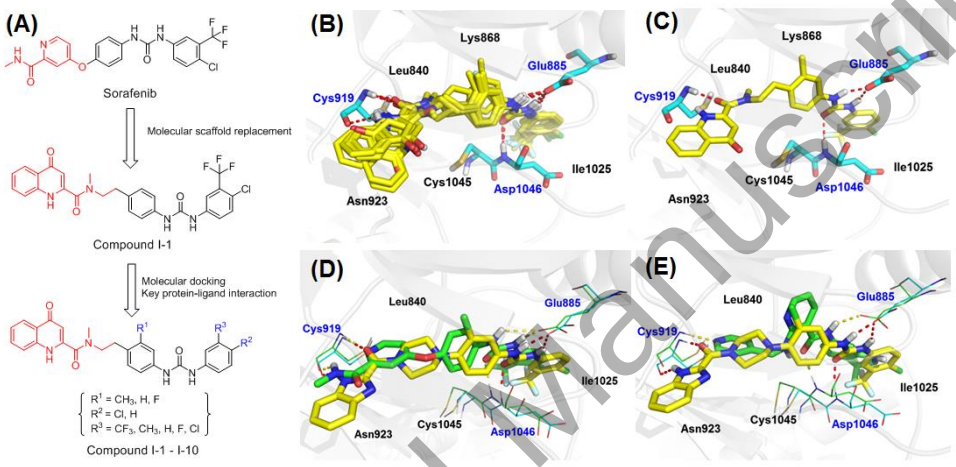

Figure 8. (A) Lead compound design and optimization workflow. (B) The docking conformation of designed compounds (PDB 3EWH); (C) The docking binding mode of the lead compound **I-1** (PDB 3EWH). (D) Comparison of the docking binding mode of **I-1** (PDB 3EWH) and sorafenib crystalized with VEGFR-2 (PDB 4ASD); (E) Comparison of the docking binding mode of **I-1** (PDB 3EWH) and motesanib crystalized with VEGFR-2 (PDB 3EFL).

As shown in **Figure 8B**, the binding mode of the 10 target compounds were similar to each other as the all occupied they three major pockets including the hinge region, DFG-motif and hydrophobic back pocket and can be regarded as type II inhibitors

like sorafenib (**Figure 8D**) and motesanib (**Figure 8E**) etc.. Similar to that of sorafenibi and motesanib, the binding mode of lead compound **I-1** (**Figure 8C)** showed that compounds **I-1** formed hydrogen bond interactions with Asp1046 and Glu885 as well as Cys919, which were recognized as some of the most critical residues for the binding of small molecules to VEGFR-2. Moreover, those target compounds also involved in the nonbonded interactions with residues like Asp1046, Ile1025, HIS1026 and Leu840 etc., which was consistent with the former protein-ligand interaction analysis. Moreover, the binding mode of these target compounds overlapped well with the cystallized conformation of known inhibitors such as sorafenib (**Figure 8D**), and motesanib (**Figure 8E**) etc., further demonstrating the posibility as potential VEGFR-2 inhibitors.

3.4 Chemistry

3.4.1 Scheme 1. Synthesis of Compounds **I-1~I-8**

Under sulfuric acid conditions, the cyano group of 2-methyl-4-nitrophenylacetonitrile alcoholysis was used to obtain ethyl phenylacetate **1**(Wojciech Dmowski, 1987). Compound **1** was reduced by $NaBH_4$ to give compound **2**(Ferri, Costa, Biancardo, Argazzi, & Bignozzi, 2007). Bromination of compound **2** provided compound **3**(Wee et al., 2009). Compound **3** was in a saturated aqueous solution of methylamine to obtain compound **4.** Compound **5** was obtained by addition reaction of aniline and dimethyl acetylenedicarboxylate(Mazzoni et al., 2010; Pandey et al., 2013). The compound **5** was cyclized in Dowtherm to give compound **6** (Mazzoni et al., 2010; Pandey et al., 2013). Under basic conditions compound **6** was

hydrolyzed to give compound **7.** Then compound **7** and compound **4** were condensed to give amide **8**(Akihiro, 2009) . Hydrogenation reduction of nitro group followed by compound **8** was to give compound **9**(Frost et al., 2010).Then compound **9** was reacted with various substituted anilines to obtain the target compounds **I-1**~**I-8** (**Scheme 1**).

Scheme 1:

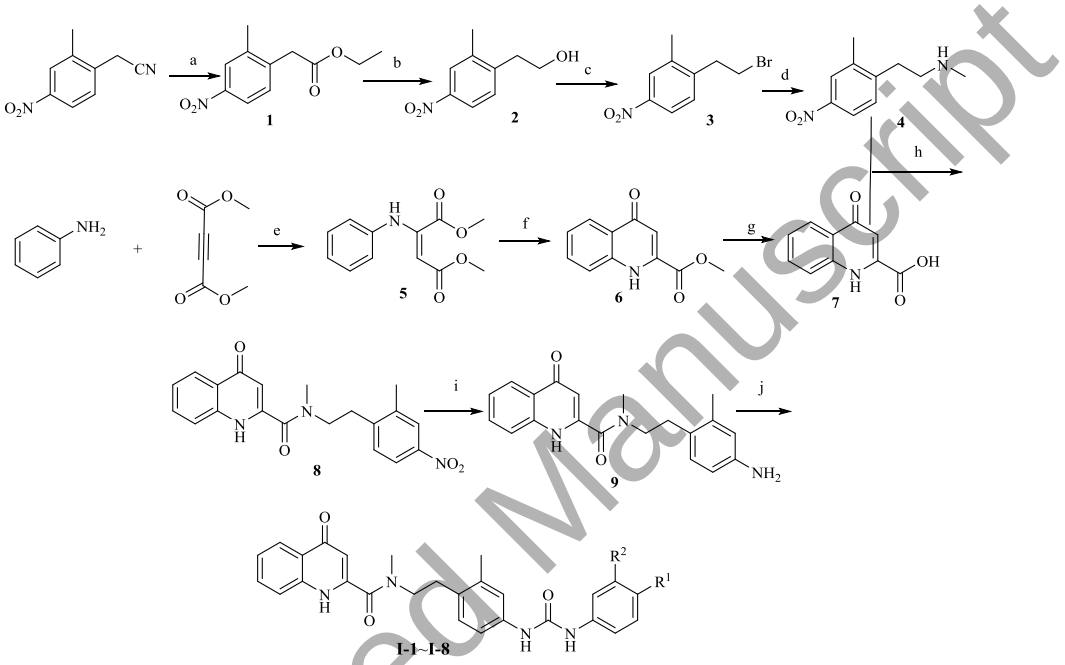

Reagents and conditions:

a) EtOH, 98%H_2SO_4, 120℃,4h; b) 4eq $NaBH_4$, EtOH, reflux, overnight; c) 1.4eq CBr_4 and 1.4 eq PPh_3, dry CH_2Cl_2, rt, 30~60min; d) 40% methylamine solution, overnight, rt; f)Dowtherm, 240℃, 30min or PPA, 130℃, 1h; g) NaOH, MeOH, rt, 2h; h) EDCI, HOBt, Et_3N, dry DMF, 5℃~rt, overnight; i) 5%Pd/C, H_2, MeOH, rt, 30min; j) aniline derivatives, CDI, dry DCM, rt.

3.4.2 Synthesis of Compound **I-9**

The synthetic process started from 1-(2-bromoethyl)-4-nitrobenzene and

compounds **10**-**12** were prepared by a method similar to that for compound **4**, **8** and **9**. Compound **12** was reacted with 4-chloro-3-trifluoromethylbenzene isocyanate to provide target compound **I-9** (**Scheme 2**).

Scheme 2:

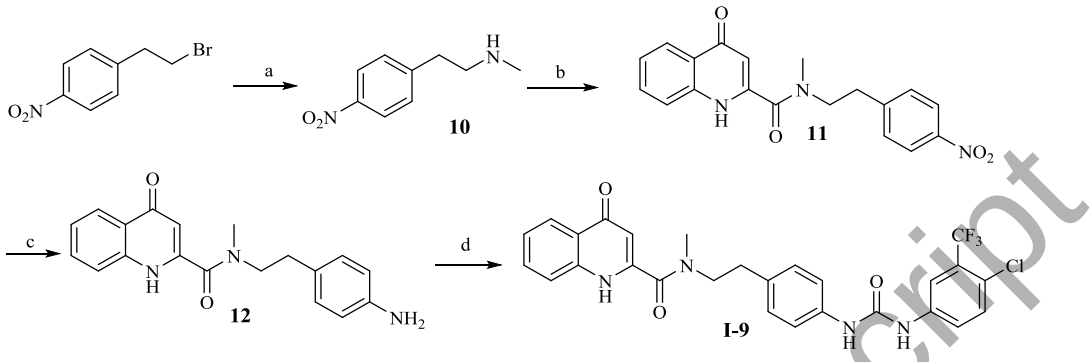

Reagents and conditions:

a) 40%methylamine water solution, rt; b) **56**, EDCI, HOBt, dry DMF; c) 5%Pd/C MeOH; d) 4-chloro-3-isocyanato-2-(trifluoromethyl)benzene, dry CH_2Cl_2, rt.

3.4.3 Synthesis of Compound **I-10**

Under basic conditions, 3, 4-Difluoronitrobenzene and ethyl cyanoacetate were reacted to provide compound **13**(Nicle, 1984). Then compound **13** was hydrolyzed and decarboxylated under acidic conditions to obtain compound **14**(Hans-Georg, 2005). Sodium borohydride reduced the ester to give compound **15**(Ferri et al., 2007). Bromination of compound **15** gave compound **16**. Compound **16** was placed in aqueous methylamine to obtain compound **17**. Compounds **18, 19** were prepared by a method similar to that of compound **8**, **9**, which were reacted with 4-chloro-3-trifluoromethylbenzene isocyanate in dichloromethane to obtain the target compound **I-10** (**Scheme 3**).

Scheme 3:

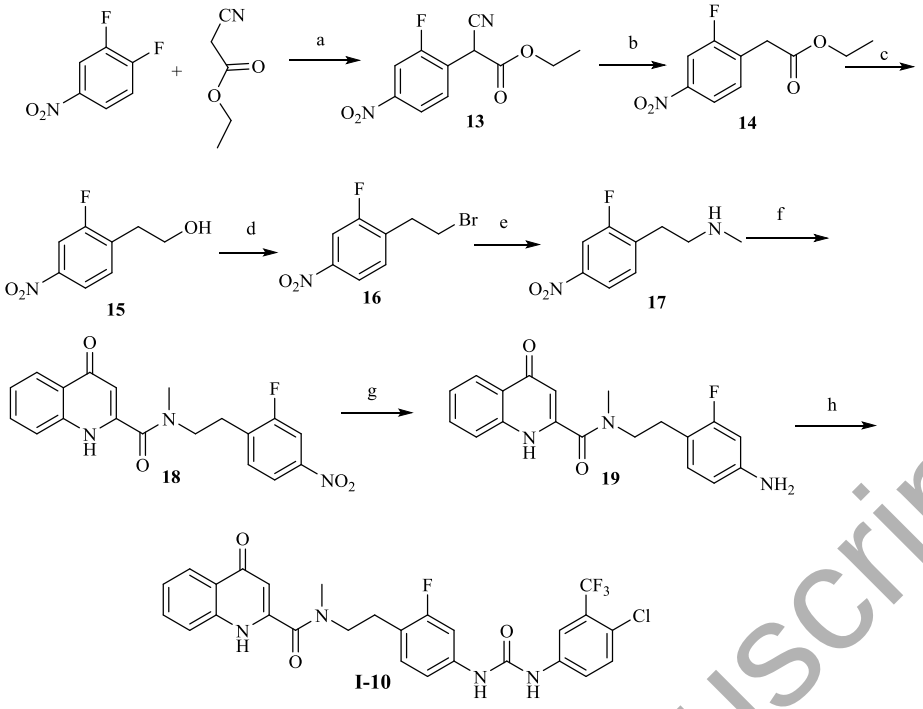

Reagents and conditions:

a) KOH, DMSO, rt, overnight; b) 98%H_2SO_4, 50%CH_3COOH, reflux, 10h; c) 4eq $NaBH_4$, EtOH, reflux, overnight; d) CBr_4/PPh_3, dry THF, rt; e) 40% methylamine water solution/THF, rt, overnight; f) **56**, EDCI, HOBt, Et_3N, dry DMF, 5℃~rt, overnight; g) 5%Pd/C, H_2, rt, 30min; h) 4-chloro-3-isocyanato-2-(trifluoromethyl)benzene, dry DCM, rt.

In summary, a total of 10 hit compounds with N-methyl-4-oxo-N-propyl-1,4-dihydroquinoline-2-carboxamide scaffold which have not been reported in the literature were synthesized (**Table 1**). At the same time, 19 synthesized intermediate compounds not reported in the literature were also obtained. All the target compounds were confirmed by IR, 1H-NMR and MS, and some of the unreported intermediates were confirmed by 1H-NMR or MS.

Table 1. The structure and the VEGFR-2 enzymatic activity as well as HepG2 and HUVEC cell activity for the target compounds.

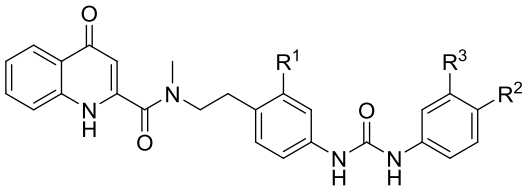

Compd.	R^1	R^2	R^3	VEGFR-2 Inhibition	HepG2 Inhibition	HUVEC (IC_{50}, μM)
I-1	CH_3	Cl	CF_3	29.01%	27.94%	57.61
I-2	CH_3	Cl	H	54.61%	32.62%	57.98
I-3	CH_3	H	CF_3	66.17%	18.60%	49.39
I-4	CH_3	Cl	Cl	68.89%	40.54%	56.98
I-5	CH_3	Cl	CH_3	62.99%	59.43%	57.47
I-6	CH_3	Cl	F	55.85%	14.34%	19.54
I-7	CH_3	H	CH_3	17.62%	-1.68%	99.15%[b]
I-8	CH_3	H	F	49.96%	-3.42%	99.51%[b]
I-9	H	Cl	CF_3	63.99%	43.07%	54.39
I-10	F	Cl	CF_3	51.93%	78.63% (33.65)[a]	54.32
Sorafenib	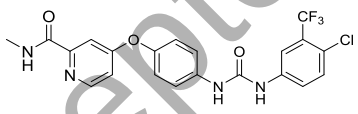			96.22% (0.045)[a]	57.55% (14.95)[a]	8.81[c]
Motesanib	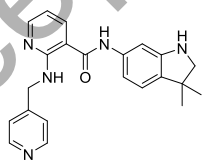			99.82% (0.020)[a]	-	33.42[c]

[a]The number in parentheses indicates the IC_{50} values of the compound and the unit is μM. [b] Represents the inhibition rate of the compound tested at the concentration of 10 μM.

3.5 Biological Activity Evaluation

The enzymatic activity against VEGFR-2 and cell antiproliferative activity for HUVEC cells as well as HepG2 cells were tested for all 10 target compounds. The results were shown in **Table 1** and **Figure 9**. It can be found that all compounds exhibited some inhibitory activity against VEGFR-2, and primary screening showed that seven compounds have an inhibition rate greater than 50%. From **Table 1** and **Figure 10**, for cellular activity evaluation, I-10 had IC_{50} values 33.65 μM against HepG2 cells, slightly inferior to the inhibitory activity of sorafenib on HepG2 cells with an IC_{50} of 14.95 μM. The activity values on the VEGFR-2 overexpression cell lines HUVEC were better than on HepG2 cell for those compounds. In the rescreening test, all compounds IC_{50} values were determined except compounds **I-7** and **I-8**. The IC_{50} values on HUVEC cell for the other 8 compounds were in the range of 19.54-57.98 μM. The most active compounds was **I-6** with IC_{50} of 19.54 μM against HUVEC cell, which was better than that of motesanib (IC_{50} = 33.42 μM) but slightly inferior to sorafenib (IC_{50} = 8.81 μM).

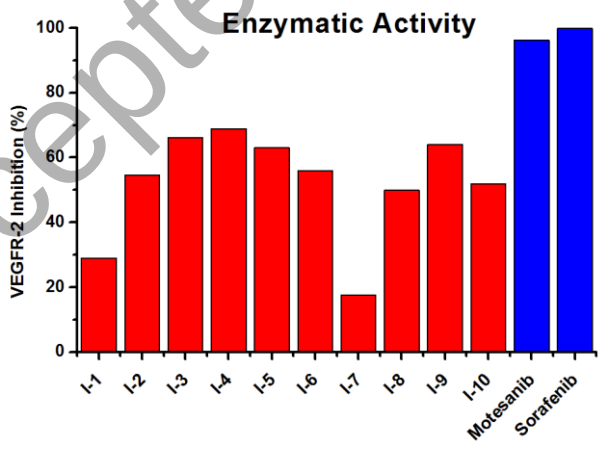

Figure 9. Enzymatic activity of the target compounds against VEGFR-2.

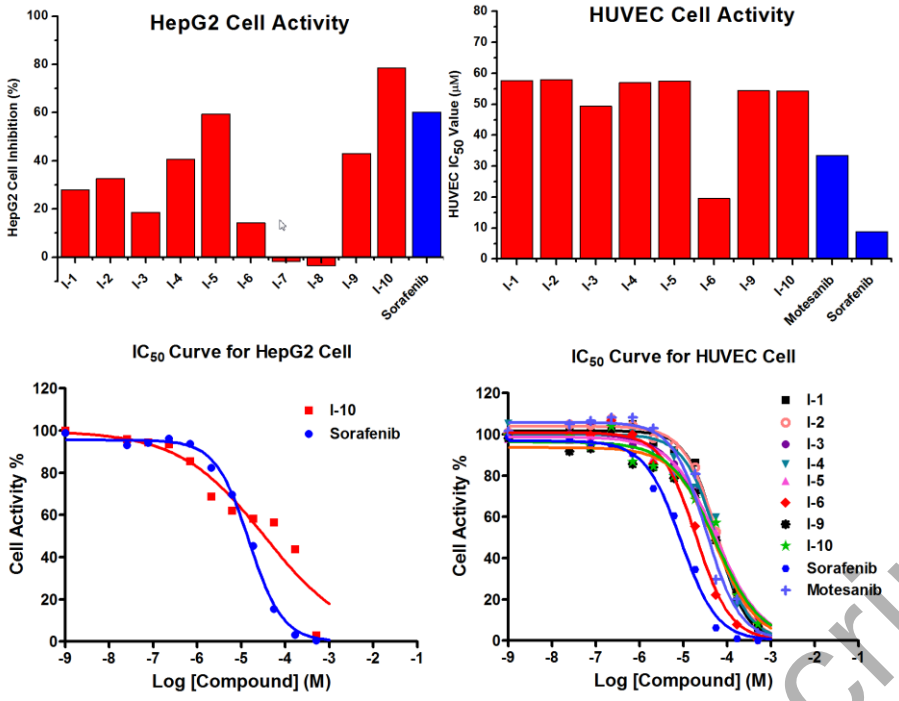

Figure 10. Antiproliferative activity of the target compounds against HepG2 and HUVEC cells and the corresponding IC_{50} curves.

In the structure-activity relationship analysis, for those compounds, when R_1 and R_2 were CH_3 and Cl respectively, bulky R_3 group like CF_3 in **I-1** would decrease the VEGFR-2 inhibitory activity according to comparison of activities for compounds **I-1**, **I-2**, **I-4**, **I-5** and **I-6**. Other groups like H, Cl, CH_3 and F substituted R_3 group showed comparable inhibition rate. When R_1 and R_3 were fixed such as R_1 and R_3 were all CH_3 like compounds **I-5** and **I-7** or R_1 as CH_3 and R_3 as F atom, R_2 preferred atoms with larger radius such as Cl atom rather than H atom. In terms of the fixed R_2 as Cl and R_3 as CF_3, comparison of the VEGFR-2 inhibition of compounds **I-1**, **I-9** and **I-10** showed that in the position of R_1, smaller atoms were favorable, which can also be confirmed by the FDA approved sorafenib and regorafenib with only H atoms in the R_1 substitution site. In this work, compounds were designed to target the VEGFR-2 and indeed showed certain inhibition toward to both VEGFR-2 and its overexpression

cell line HUVEC. For example, compound I-6 with the best HUVEC cell activity of 19.54 μM, had an VEGFR-2 inhibition rate of 55.85%. While for compound I-7 with the least VEGFR-2 inhibition rate of only 17.62%, its performance on HepG2 (-1.68%) and HUVEC (99.15%, IC_{50} values not determined) were also not favorable. However, it was worth noting that enzymatic activity and cell activity were not always in the same trend. For example, compound **I-1** achieved only 29.01% inhibition rate on VEGFR-2 enzymatic activity but obtained a IC_{50} value of 57.61 μM on HUVEC cell activity, while compound I-8 obtained opposite results. This phenomenon happens sometimes as they are large amount of factors that can influence cell activity such as the compound cell permeability which may be affected by the physiochemical properties of the compounds or the multi-target effect.

4. CONCLUSIONS

In this paper, a comprehensive binding hot spot and protein-ligand interaction analysis were conducted on all the available VEGFR-2 crystal structures. Results showed that Asp1046, Ile1025, HIS1026, Cys919 and Lys868 are the most important residues for Hbonded interaction, while for His1026, Asp1046, Glu885, Ile1025 and Leu840 play critical role for the nonbonded interactions. Furthermore, structure-based virtual screening were applied to a fragment-based compound database and a total of 10 target compounds based on the N-methyl-4-oxo-N-propyl-1,4-dihydroquinoline-2-carboxamide scaffold that have not been reported in the literature. Enzymatic activity evaluation showed that the synthesized compounds exerted certain enzymatic activity against VEGFR-2 but was

inferior to that of the positive drug sorafenib and motesanib. However, the cell activity showed that compound I-10 showed moderate HepG2 cell inhibitory activity with an IC_{50} value of 33.65 μM, and eight compounds exhibited moderate or higher HUVEC inhibitory activity in the range of 19.54-57.98 μM. Particularly, the HUVEC inhibitory activity of compound I-6 (IC_{50} = 19.54 μM) outperformed the positive control motesanib (IC_{50} = 33.42 μM), but was slightly inferior to that of sorafenib (IC_{50} = 8.81 μM). This type of novel VEGFR-2 inhibitors can serve as starting points for further optimization and development in cancer treatment.

ASSOCIATE CONTENT

Supplementary Materials

The details of the synthesis process and MS data for the target compounds as well as the intermediates. **Table S1**. Number of probe clusters detected for each consensus site of the 38 VEGFR-2 crystal structures based on FTMap analysis. **Table S2**. Hbonded interaction frequency values for all 38 VEGFR-2 complexes. **Table S3**. Nonbonded interaction frequency values for all 38 VEGFR-2 complexes.

AUTHOR INFORMATION

Corresponding Authors

For Haichun Liu: Tel.: +86-25-86185163. Fax: +86-25-86185182. E-mail: tuna888@126.com.

For Yadong Chen: Tel.: +86-25-86185163. Fax: +86-25-86185182. E-mail: ydchen@cpu.edu.cn.

ORCID

For Haichun Liu: 0000-0003-0164-3502

Author Contributions

The manuscript was written through contributions of all authors. Yanmin Zhang and Mingliang Zhang contributed equally to this work and should be considered as cofirst authors. All authors have given approval to the final version of the manuscript.

Conflict of interest

The authors declare no competing financial interest.

ACKNOWLEDGMENTS

This work was financially supported by National Natural Science Foundation of China (No. 81803370), Natural Science Foundation of Jiangsu Province (No. BK20180559), State Key Laboratory Innovation Research and Cultivation Fund (No. SKLNMZZCX201812), and "Double World-classes" Construction Program of China Pharmaceutical University (No. CPU2018GF02).

ABBREVIATIONS USED

VEGF-A, vascular endothelial growth factor A; VEGFR, vascular endothelial growth factor receptor; VEGFR-2, vascular endothelial growth factor receptor-2; DFG, Asp-Phe-Gly; $IC_{50,}$ 50% inhibition activity; HUVEC, human umbilical vein endothelial cells; HepG2, liver hepatocellular carcinoma; HTRF, homogeneous time-resolved fluorescence; TLC, thin-layer chromatography

REFERENCE

Akihiro, F. (2009). Preparation of novel 2-phenylpyrrole derivatives as glucokinase activators. *WO2009099080*.

Baell, J. B., & Holloway, G. A. (2010). New substructure filters for removal of pan assay interference compounds (pains) from screening libraries and for their exclusion in bioassays. *Journal of*

Medicinal Chemistry, 53, 2719-2740. doi:10.1021/jm901137j

Barouch-Bentov, R., & Sauer, K. (2011). Mechanisms of drug resistance in kinases. *Expert opinion on investigational drugs, 20*, 153-208.

Bergmann, R., Linusson, A., & Zamora, I. (2007). Shop: Scaffold hopping by grid-based similarity searches. *Journal of Medicinal Chemistry, 50*, 2708-2717. doi:10.1021/jm061259g

Bian, Y., & Xie, X. S. (2018). Computational fragment-based drug design: Current trends, strategies, and applications. *Aaps Journal, 20*, 59. doi:10.1208/s12248-018-0216-7

Brenke, R., Kozakov, D., Chuang, G.-Y., Beglov, D., Hall, D., Landon, M. R., . . . Vajda, S. (2009). Fragment-based identification of druggable 'hot spots' of proteins using fourier domain correlation techniques. *Bioinformatics, 25*, 621-627. doi:10.1093/bioinformatics/btp036

Davis, M. I., Hunt, J. P., Herrgard, S., Ciceri, P., Wodicka, L. M., Pallares, G., . . . Zarrinkar, P. P. (2011). Comprehensive analysis of kinase inhibitor selectivity. *Nature Biotechnology, 29*, 1046-1051.

Dima, K., David R, H., Gwo-Yu, C., Regina, C., Ryan, B., Laurie E, G., . . . Sandor, V. (2011). Structural conservation of druggable hot spots in protein-protein interfaces. *Proceedings of the National Academy of Sciences of the United States of America, 108*, 13528-13533. doi:10.1073/pnas.1101835108

Ding, K., Kong, X., Wang, J., Lu, L., Zhou, W., Zhan, T., . . . Zhuang, S. (2017). Side chains of parabens modulate antiandrogenic activity: In vitro and molecular docking studies. *Environmental Science & Technology, 51*, 6452-6460. doi:10.1021/acs.est.7b00951

Ertl, P., Rohde, B., & Selzer, P. (2000). Fast calculation of molecular polar surface area as a sum of fragment-based contributions and its application to the prediction of drug transport properties. *Journal of Medicinal Chemistry, 43*, 3714-3717. doi:10.1021/jm000942e

Ferrara, N. (2004). Vascular endothelial growth factor as a target for anticancer therapy. *The oncologist, 9*, 2-10. doi:10.1634/theoncologist.9-suppl_1-2

Ferrara, N., Hillan, K. J., Gerber, H.-P., & Novotny, W. (2004). Discovery and development of bevacizumab, an anti-vegf antibody for treating cancer. *Nature Reviews Drug Discovery, 3*, 391-400. doi:10.1038/nrd1381

Ferri, V., Costa, E., Biancardo, M., Argazzi, R., & Bignozzi, C. A. (2007). Electrochromic properties of mixed valence binuclear ruthenium complexes adsorbed on nanocrystalline sno2 films. *Inorganica Chimica Acta, 360*, 1131-1137. doi:10.1016/j.ica.2006.08.040

Folkman, J., & D'Amore, P. A. (1996). Blood vessel formation: What is its molecular basis? *Cell, 87*, 1153-1155. doi:10.1016/S0092-8674(00)81810-3

Frost, J. M., Dart, M. J., Tietje, K. R., Garrison, T. R., Grayson, G. K., Daza, A. V., . . . Meyer, M. D. (2010). Indol-3-ylcycloalkyl ketones: Effects of n1 substituted indole side chain variations on cb2 cannabinoid receptor activity. *Journal of Medicinal Chemistry, 53*, 295-315. doi:10.1021/jm901214q

Hanahan, D., & Folkman, J. (1996). Patterns and emerging mechanisms of the angiogenic switch during tumorigenesis. *Cell, 86*, 353-364. doi:10.1016/S0092-8674(00)80108-7

Hans-Georg, C. (2005). 1h-imidazo[4,5-c]quinoline derivatives in the treatment of protein kinase department diseases. *WO2005054238*.

Holmes, K., Roberts, O. L., Thomas, A. M., & Cross, M. J. (2007). Vascular endothelial growth factor receptor-2: Structure, function, intracellular signalling and therapeutic inhibition. *Cellular Signalling, 19*, 2003-2012. doi:10.1016/j.cellsig.2007.05.013

Ivy, S. P., Wick, J. Y., & Kaufman, B. M. (2009). An overview of small-molecule inhibitors of vegfr signaling. *Nature reviews Clinical oncology, 6*, 569-579. doi:10.1038/nrclinonc.2009.130

Kappert, K., Peters, K. G., Böhmer, F. D., & Östman, A. (2005). Tyrosine phosphatases in vessel wall signaling. *Cardiovascular Research, 65*, 587-598. doi:10.1016/j.cardiores.2004.08.016

Kiselyov, A., Balakin, K. V., & Tkachenko, S. E. (2007). Vegf/vegfr signalling as a target for inhibiting angiogenesis. *Expert opinion on investigational drugs, 16*, 83-107. doi:10.1517/13543784.2011.546344

Klagsbrun, M., & Moses, M. A. (1999). Molecular angiogenesis. *Chemistry & Biology, 6*, R217-R224.

Koch, S., Tugues, S., Li, X., Gualandi, L., & Claesson-Welsh, L. (2011). Signal transduction by vascular endothelial growth factor receptors. *Biochemical Journal, 437*, 169-183. doi:10.1042/BJ20110301

Labute, P. (2009). Protonate3d: Assignment of ionization states and hydrogen coordinates to macromolecular structures. *Proteins: Structure, Function, and Bioinformatics, 75*, 187-205. doi:10.1002/prot.22234

Landon, M., Lancia-Dr, J. Y., J, Thiel, S., & Vajda, S. (2007). Identification of hot spots within druggable binding regions by computational solvent mapping of proteins. *Journal of Medicinal Chemistry, 50*, 1231-1240. doi:10.1021/jm061134b

Li, B., Sharpe, E. E., Maupin, A. B., Teleron, A. A., Pyle, A. L., Carmeliet, P., & Young, P. P. (2006). Vegf and plgf promote adult vasculogenesis by enhancing epc recruitment and vessel formation at the site of tumor neovascularization. *The FASEB Journal, 20*, 1495-1497. doi:10.1096/fj.05-5137fje

Lu, L., Zhan, T., Ma, M., Xu, C., Wang, J., Zhang, C., . . . Zhuang, S. (2018). Thyroid disruption by bisphenol s analogues via thyroid hormone receptor β: In vitro, in vivo and molecular dynamics simulation study. *Environmental Science & Technology, 52*, 6617-6625. doi:10.1021/acs.est.8b00776

Mazzoni, O., Esposito, G., Diurno, M. V., Brancaccio, D., Carotenuto, A., Grieco, P., . . . Filippelli, W. (2010). Synthesis and pharmacological evaluation of some 4-oxo-quinoline-2-carboxylic acid derivatives as anti-inflammatory and analgesic agents. *Archiv der Pharmazie, 343*, 561-569. doi:10.1002/ardp.201000016

Morabito, A., De Maio, E., Di Maio, M., Normanno, N., & Perrone, F. (2006). Tyrosine kinase inhibitors of vascular endothelial growth factor receptors in clinical trials: Current status and future directions. *The Oncologist, 11*, 753-764. doi:10.1634/theoncologist.11-7-753

Musumeci, F., Radi, M., Brullo, C., & Schenone, S. (2012). Vascular endothelial growth factor (vegf) receptors: Drugs and new inhibitors. *Journal of Medicinal Chemistry, 55*, 10797-10822. doi:10.1021/jm301085w

Ngan, C. H., Bohnuud, T., Mottarella, S. E., Beglov, D., Villar, E. A., Hall, D. R., . . . Vajda, S. (2012). Ftmap: Extended protein mapping with user-selected probe molecules. *Nucleic Acids Research, 40*, W271-275. doi:10.1093/nar/gks441

Nicle, m. (1984). High diastereoselectivity in the reaction of a-amino nitriles bearing an (s)(+)-2-methoxymethylpyrrolidine group with grignard reagents. *Journal of the Chemical Society, Chemical Communications, 15*, 40-41. doi:10.1002/chin.198419197

Pandey, A. K., Sharma, R., Shivahare, R., Arora, A., Rastogi, N., Gupta, S., & Chauhan, P. M. S. (2013). Synthesis of perspicamide a and related diverse analogues: Their bioevaluation as potent antileishmanial agents. *Journal of Organic Chemistry, 78*, 1534-1546. doi:10.1021/jo3025626

Pei, J., Wang, Q., Liu, Z., Li, Q., Yang, K., & Lai, L. (2006). Psi‐dock: Towards highly efficient and accurate flexible ligand docking. *Proteins: Structure, Function, and Bioinformatics, 62*, 934-946. doi:10.1002/prot.20790

Risau, W. (1997). Mechanisms of angiogenesis. *Nature, 386*, 671. doi:10.1007/b137088

Roth, G. J., Heckel, A., Colbatzky, F., Handschuh, S., Kley, J. r., Lehmann-Lintz, T., . . . Hilberg, F. (2009). Design, synthesis, and evaluation of indolinones as triple angiokinase inhibitors and the discovery of a highly specific 6-methoxycarbonyl-substituted indolinone (bibf 1120). *Journal of Medicinal Chemistry, 52*, 4466-4480. doi:10.1021/jm900431g

Roviello, G., Ravelli, A., Polom, K., Petrioli, R., Marano, L., Marrelli, D., . . . Generali, D. (2016). Apatinib: A novel receptor tyrosine kinase inhibitor for the treatment of gastric cancer. *Cancer Letters, 372*, 187-191. doi:10.1016/j.canlet.2016.01.014

Schrodinger, L. (2011). Schrodinger software suite. *New York: Schrödinger, LLC*.

Tardieu, J.-L. (2007). Htrf® kinase™ tk: A new solution for tyrosine kinase screening. *Nature Methods, 4*, i-ii.

Wee, S., Jagani, Z., Xiang, K. X., Loo, A., Dorsch, M., Yao, Y.-M., . . . Stegmeier, F. (2009). Pi3k pathway activation mediates resistance to mek inhibitors in kras mutant cancers. *Cancer Research, 69*, 4286-4293. doi:10.1158/0008-5472.can-08-4765

Wildman, S. A., & Crippen, G. M. (1999). Prediction of physicochemical parameters by atomic contributions. *Journal of Chemical Information and Computer Sciences, 39*, 868-873. doi:10.1021/ci990307l

Wojciech Dmowski, A. H. (1987). Trifluoromethanethiolate ion. Part 2. Nucleophilic substitution in pentafluoropyridine. Synthesis and characteristics of trifluoromethylthio and trifluoromethylsulphonyl derivatives. *Journal of the Chemical Society. Perkin Transactions 1, 10*, 2119-2124. doi:10.1039/P19870002119

Yang, W., Chen, Y., Zhou, X., Gu, Y., Qian, W., Zhang, F., . . . Tang, W. (2015). Design, synthesis and biological evaluation of bis-aryl ureas and amides based on 2-amino-3-purinylpyridine scaffold as dfg-out b-raf kinase inhibitors. *European Journal of Medicinal Chemistry, 89*, 581-596. doi:10.1016/j.ejmech.2014.10.039

Zhang, Y., Chen, Y., Zhang, D., Wang, L., Lu, T., & Jiao, Y. (2017). Discovery of novel potent vegfr-2 inhibitors exerting significant antiproliferative activity against cancer cell lines. *Journal of Medicinal Chemistry, 61*, 140-157. doi:10.1021/acs.jmedchem.7b01091

Zhang, Y., Liu, H., Jiao, Y., Yuan, H., Wang, F., Lu, S., . . . Lu, T. (2012). De novo design of n-(pyridin-4-ylmethyl)aniline derivatives as kdr inhibitors: 3d-qsar, molecular fragment replacement, protein-ligand interaction fingerprint, and admet prediction. *Molecular Diversity, 16*, 787-802. doi:10.1007/s11030-012-9405-y

Zhang, Y., Yang, S., Jiao, Y., Liu, H., Yuan, H., Lu, S., . . . Lu, T. (2013). An integrated virtual screening approach for vegfr-2 inhibitors. *Journal of Chemical Information and Modeling, 53*, 3163-3177. doi:10.1021/ci400429g

Zhang, Y., Zhang, D., Tian, H., Jiao, Y., Shi, Z., Ran, T., . . . Qiao, X. (2016). Identification of covalent binding sites targeting cysteines based on computational approaches. *Molecular Pharmaceutics, 13*, 3106-3118. doi:10.1021/acs.molpharmaceut.6b00302